Carboxylate-functionalized dragon fruit peel powder as an effective adsorbent for the removal of Rhodamine B (cationic dye) from aqueous solution: adsorption behavior and mechanism

Munagapati Venkata Subbaiah, Hsin-Yu Wen, Anjani R. K. Gollakota, Jet-Chau Wen, Chi-Min Shu, Kun-Yi Andrew Lin, Yarramuthi Vijaya, Dong-Su Kim & Jhy-Horng Wen

Published online: 27 Apr 2022.

Submit your article to this journal ↗

Article views: 82

View related articles ↗

View Crossmark data ↗

Taylor & Francis
Taylor & Francis Group

Check for updates

Carboxylate-functionalized dragon fruit peel powder as an effective adsorbent for the removal of Rhodamine B (cationic dye) from aqueous solution: adsorption behavior and mechanism

Munagapati Venkata Subbaiah[a], Hsin-Yu Wen[b], Anjani R. K. Gollakota[c], Jet-Chau Wen[a,c], Chi-Min Shu[c] (ID), Kun-Yi Andrew Lin[d], Yarramuthi Vijaya[e], Dong-Su Kim[f], and Jhy-Horng Wen[g]

[a]Research Centre for Soil & Water Resources and Natural Disaster Prevention (SWAN), National Yunlin University of Science and Technology, Douliou, Taiwan; [b]Department of Pathology, West China Hospital, Sichuan University, Chengdu, China; [c]Department of Safety, Health, and Environmental Engineering, National Yunlin University of Science and Technology, Douliou, Taiwan; [d]Department of Environmental Engineering, National Chung Hsing University, Taichung, Taiwan; [e]Department of Chemistry, Vikrama Simhapuri University, Nellore, India; [f]Department of Environmental Science and Engineering, Ewha Womans University, Seoul, Korea; [g]Department of Electrical Engineering, Tunghai University, Taichung, Taiwan

ABSTRACT

In this study, we used a simple and low-toxicity chemical treatment to make a carboxylate-functionalized dragon fruit peel powder (CF-DFPP) from dragon fruit peel to improve its capacity for adsorbing Rhodamine B (RhB) from an aqueous medium. Field Emission-Scanning Electron Microscopy/Energy-Dispersive X-ray (FE-SEM/EDX), point of zero charges (pH$_{PZC}$), Brunauer-Emmett-Teller (BET), and Fourier Transform Infrared (FT-IR) analyses were performed to characterize the adsorbent materials. The adsorption performance and mechanism for the removal of RhB were examined. The kinetic, isotherm and thermodynamic parameters were employed to evaluate the adsorption mechanism. Compared to other models, the Langmuir isotherm and PSO kinetic models better defined the experimental data. CF-DFPP adsorbent exhibited a maximum adsorption efficiency of 228.7 mg/g at 298 K for RhB adsorption. Thermodynamic analysis revealed that the adsorption of RhB by CF-DFPP was spontaneous ($\Delta G^o < 0$) and exothermic ($\Delta H^o < 0$) nature of the process. Different eluting agents were used in desorption tests, and NaOH was revealed to have greater desorption efficiency (96.8%). Furthermore, regeneration examinations revealed that the biosorbent could effectively retain RhB, even after six adsorption/desorption cycles. These findings demonstrated that the CF-DFPP might be a novel material for removing RhB from an aqueous medium.

GRAPHICAL ABSTRACT
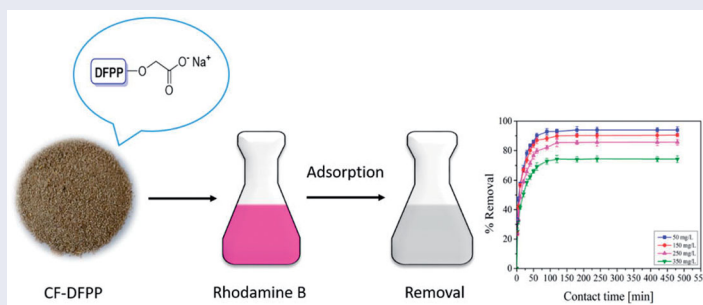
NOVELTY STATEMENT

To improve the efficiency of adsorbing Rhodamine B (RhB) from aqueous streams, a low-toxic carboxylate-functionalized (CF) dragon fruit peel powder sorbent material was synthesized. Following the chemical transfer, the surface area of DFPP was increased dramatically from 4.49 to 23.6 m^2/g, resulting in a higher adsorption efficiency and reusability than previously reported. The choice of the CF significantly increases the number of anions and attracts the positively charged RhB, increasing the sorption tendency. Despite the abundance of material on the direct use of dragon fruit peel as an adsorbent, no research has been done on the adsorbent surface modification. As a result, an effort has been made to add a novel adsorbent to the adsorbents database in this approach.

Nomenclature: C_o & C_e: starting & equilibrium RhB solution concentration; C_{Ae}: solid phase concentration at equilibrium; k_1 & k_2: constant of the PFO and PSO; K_c: distribution constant; K_f: Freundlich constant related to adsorption capacity; K_L: adsorption energy constant of the Langmuir isotherm; K: constant related to sorption energy; M: mass of CF-DFPP; n: Freundlich constant related to the adsorption intensity; $1/n$: heterogeneity factor; PFO: pseudo-first-order; PSO: pseudo-second-order; q_e: adsorption equilibrium amount; $q_{e,cal}$ & $q_{e,exp}$: calculate & experimental adsorption amounts; q_{e1} & q_{e2}: amount of dye adsorbed at equilibrium; q_t: adsorption rate on at time; q_{max}: maximum adsorption quantity; q_s: theoretical saturation uptake of the D-R model; R: gas constant (8.314 kJ/mol K); t: contact time, min; T: temperature (K); V: RhB solution volume (L). *Greek letters:*; α: initial adsorption rate of Elovich model; β: desorption constant; ε: Polanyi potential.

Introduction

Water, a natural solvent, is known for its universal solubility for most known substances. Industrial, agricultural, and domestic activities produce contaminants that are readily mixed with natural water bodies, leading to their easy contamination. This water contamination takes a toll on the humans and other living beings dependent on these water bodies (Vigneshwaran *et al.* 2021b). Various dyes released from the textile industry are significant contributors to environmental pollution (Sharma *et al.* 2015, 2017). An enormous amount of dyes is produced worldwide for the textile industry, among which 10–15% are directly contaminating the water bodies creating environmental risk and not pleasing for human consumption (Mu and Wang 2016; Naushad *et al.* 2019). Dyes are resistant to several conventional water treatments because of their complex chemical structure and weak biodegradability (Khorasani and Shojaosadati 2019). Rhodamine B (RhB) is a water-soluble cationic dye of the xanthan type that is extensively used in the leather, dyeing, textile industries, and biomedical laboratories (Cheng *et al.* 2018). RhB is also known to cause cancers and eye, skin, respiratory, and neuro-related problems to its exposures (Sadegh *et al.* 2021). Therefore, removing RhB from the water bodies is an immediate need of the hour.

Several treatment techniques such as advanced oxidation processes, coagulation, photochemical degradation, chemical oxidation, Fenton-biological degradation, membrane filtration, sedimentation, ozonolysis, electrochemical processes, biodegradation, etc., have been applied for the elimination of RhB from wastewater (Nazir *et al.* 2021). However, these approaches have several environmental and economic drawbacks, such as generation of secondary pollutants, inadequate removal efficiency, complex treatment techniques, operations delay, high costs, and oxidizing agent dependence. On the contrary, adsorption technology is a superior alternative treatment technique due to its cheap cost, ease of operation conditions, fast, biosorbents diversity, ease of regenerating, inertness to materials, high efficiency, and environmentally friendly compared to other treatment techniques (Egbosiuba *et al.* 2020).

Dragon fruit scientifically termed *Hylocereus undatus* is widely cultivated in many Southeast Asian countries. Dragon fruits also possess many phytonutrients with many beneficial effects, such as they can heal wounds, strengthening the immune system, lower the risk of prostate cancer, improving eyesight, etc. (Ahmad *et al.* 2021). Dragon fruit consumption also produces lots of biodegradable wastes in the form of their outer skin (peels). These dragon fruits are available in red/yellowish flesh with numerous small seeds, edible, and the peels are non-edible and usually discarded. In the present study, these waste materials (peels) were taken as adsorbent material to remove dyes from an aqueous solution since they are available at no cost, reducing disposal costs.

In literature, a variety of agricultural waste materials have been successfully employed as a biosorbent for the elimination of dyes, such as barberry stem (Kamranifar *et al.* 2018), bottle ground peel (Palamthodi and Lele 2016), pineapple plant stem (Chan *et al.* 2016), pomegranate peel (Gündüz and Bayrak 2017), Formosa papaya seed powder (Pavan *et al.* 2014), *Antigonon leptopus* leaf powder (Devi *et al.* 2020), cabbage waste powder (Wekoye *et al.* 2020), *Moringa oleifera* Lam. seeds (Dos Santos Escobar *et al.* 2021) and others. However, the utilization of these unmodified agricultural wastes for adsorption is restricted by a variety of restrictions such as limited surface area, lesser surface factional groups, low removal ability, fewer active sites for sorption, etc. (Wang *et al.* 2019). Therefore, there is a definite need for modification with other materials. There are several methods that exist for modifying biomass wastes for adsorption, including doping with photocatalysts, coupling with two or more biosorbents to form a composite, magnetization, functionalization with exogenous active functional groups, chemical treatments, etc. All these methods could improve adsorption efficiencies through the enhancing or activation of surface functional groups in the agricultural by-products. Several researchers developed modified agricultural wastes that have been effectively used in the separation of dyes from aqueous solutions, some of which are quaternary amine-modified orange peel (Munagapati *et al.* 2019), calcined magnetic orange peel (Shehzad *et al.* 2018), acid-washed black cumin seed powder (Siddiqui *et al.* 2018), magnetite nanoparticles loaded solanum tuberosum peel (Akpomie and Conradie 2021), surface modified *Delonix regia* seed (Saravanan *et al.* 2020), chemically treated *Lawsonia inermis* seeds powder (Ahmad and Ansari 2020), and NaOH modified areca nut husk (Sukla Baidya and Kumar 2021), etc. CF-DFPP was selected as an biosorbent to remove RhB from an aqueous phase in the current investigation. However, according to our knowledge and literature review, no study about RhB removal utilizing CF-DFPP.

The goal of this work was to synthesize carboxylate-functionalized dragon fruit peel powder (CF-DFPP) utilizing monochloroacetic acid as an etherifying agent in a simple and low-toxic procedure. DFPP, CF-DFPP, and RhB loaded CF-DFPP were characterized by FE-SEM/EDX, BET-BJH, pH$_{PZC}$, and FT-IR analysis. The effect of temperature,

solution pH, starting dye concentration, adsorbent dosage, adsorption time, and stirring speed were examined to investigate the adsorption behavior of RhB onto CF-DFPP. The properties like adsorption isotherms, kinetics, and thermodynamics were also determined using the experimental batch method. The regeneration experiments were also performed to determine whether this adsorbent could be reused.

Materials and methods

Materials

The peels of dragon fruit were gathered from a local market in Douliu, Taiwan. Rhodamine B (RhB) was acquired from Sigma-Aldrich (USA), was used as adsorbate. The properties and characteristics of the RhB dye are presented in Table 1. All additional chemicals/reagents were of analytical quality and were utilized just as they were received, with no further purification. An exactly weighed amount of the RhB dye was dissolved in deionized (DI) water (< 18 MOhm-cm) to prepare stock and the diluted dye solutions.

CF-DFPP preparation

The collected dragon fruit peels were cleaned with DI water multiple times to remove adhering filth and dust particles and then dried at 343 K in an oven for 48 h. The dried peels were ground into a mechanical grinder to get a fine powder and sieved to get a uniform particle size (0.35 mm). The fine power is named dragon fruit peel powder (DFPP).

The prior obtained powder was synthesized as follows, 10.0 g of DFPP and 100 mL of 80% ethanol were taken in a glass beaker (250 mL). Afterwards, an aliquot of NaOH (20%, 22.2 mL) was added to this solution, followed by monochloroacetic acid (10.75 g). Then added a magnetic bar to the beaker, the reaction mixture was mixed using a magnetic stirrer at 200 rpm for 3 h at 353 K. Following the reaction, the treated material was filtered, washed with ethanol (80%) until the pH was stable at 7.0, and then dried in an oven at 343 K for 7 h to get CF-DFPP. The schematic representation of adsorbent preparation is as follows:
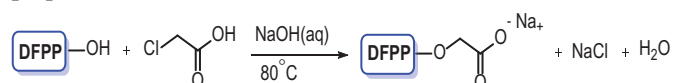
Instrumentation

The characteristics of the samples were examined using various instrumental analyses. The functional groups present in the DFPP, CF-DFPP, and RhB loaded CF-CFPP were recorded using FT-IR spectrometer by KBr pellet procedure using the range 400.0–4,000 cm^{-1} by Nicolet iS-10 model. 10.0 mg of the adsorbent was combined and mashed with 100.0 mg of KBr to make a pellet for IR spectral measurements. The elemental composition and surface morphology of the DEPP, CF-DFPP, and RhB loaded CF-DFPP was analyzed by FE-SEM (JSM-7610F plus, JEOL, Japan) coupled with an EDX spectrometer. Before the test, the samples were coated with a homogeneous layer of gold in a sputter coater for 2 min and then loaded onto a copper substrate. The surface area of the DFPP and CF-DFPP was quantified from the N_2 adsorption/desorption isotherms on the basis of the BET method using Quantachrome NOVA 2,000 surface area analyzer at 77 K. Before the analysis; each sample was degassed at 378 K for 12 h. The pore radius and pore volume were evaluated by the BJH method. The pH$_{PZC}$ (point of zero charges) was determined to ascertain the surface charge of CF-DFPP.

Batch adsorption experiments

The batch mode adsorption tests are performed in 30 mL of RhB solution with different adsorbent weights ranging from 10 to 70 mg to find the best weight that will be employed in this study. Various contact periods (0–480 min) were explored in order to estimate the contact time required to attain adsorption equilibrium and to conduct the kinetic analysis by investigating the PFO, PSO, and Elovich kinetic models. By varying the concentration of RhB from 50 to 400 mg/L, the starting dye concentration impact was examined. This study allowed plotting the adsorption isotherms of Dubinin-Radushkevich (D-R), Freundlich, and Langmuir. The effect of temperature is then investigated by varying it from 298 to 328 K. Using these data, we were able to determine the following thermodynamic variables (ΔH^o, ΔS^o, and ΔG^o). The impact of altering the pH of the solution from 1.0 to 10.0 was evaluated by adding a few drops of NaOH (0.1 M) and HCl (0.1 M) before adsorbent addition. All of the samples were removed from the incubator after the specified time span. To get clear solutions, the adsorbent samples were removed from the solution by centrifugation at 8,000 rpm for 10 min. The concentration of the final supernatant was calculated by measuring its absorbance using a UV-Vis (Ultraviolet-Visible) spectrophotometer. The tests were repeated in duplicate, and the average value was taken. The amount of dye adsorbed per unit mass of sorbent at equilibrium, q_e (mg/g), and removal rate, R (%), were

Table 1. Characteristics of Rhodamine B.

Characteristics	Rhodamine B
Chemical names	Basic violet 10, Brilliant pink B, Tetraethylrhodamine
IUPAC name	[9-(2-carboxyphenyl)-6-diethylamino-3-xanthenylidene]-diethylammonium chloride
C.I number	45170
Application class	Cationic dye
λ_{max}	554 nm
Molecular formula	$C_{28}H_{31}N_2O_3Cl$
Molecular weight	479.02 g/mol
Chemical structure	

obtained using the following Equations.

$$q_e(mg/g) = \frac{[C_o - C_e]V}{M} \qquad (1)$$

$$R\% = \frac{C_o - C_e}{C_o} \times 100 \qquad (2)$$

Desorption and reusability studies

After adsorption, the RhB adsorbed CF-DFPP adsorbent was used for desorption studies. The desorbing eluents used in this study were 0.1 M NaCl, H_2O, 0.1 M NaOH, 0.1 M CH_3COOH, and 0.1 M HCl. After each adsorption cycle, 40 mg of dried RhB loaded CF-DFPP was added to 30 mL of eluent and stirred for 120 min at 298 K to achieve complete desorption. After then, the mixture was centrifuged and the residual dye concentration in the supernatant was evaluated by using a UV-Vis spectrophotometer. The adsorbent was cleaned with DI water until neutral pH and then oven-dried at 60 °C for 4 h. Then, the desorbed adsorbent was used for the subsequent adsorption/desorption cycle. Each experiment was repeated under the same conditions two times and the average value was taken. The regeneration efficiency was determined using Equation (2), while the desorption efficiency was computed using the following relationship:

$$Desorption\ (\%) = \frac{RhB\ desorbed}{RhB\ adsorbed} \times 100 \qquad (3)$$

Results and discussion

Characterization of the adsorbent

FT-IR analysis

The FT-IR spectrum of DFPP, CF-DFPP, and RhB loaded CF-DFPP are displayed in Figure 1 to identify some of the distinctive functional groups present on the surface of the adsorbents. In the DFPP spectrum (Figure 1a), the strong and wide absorption peak that appears in the region of $3,409\ cm^{-1}$ was ascribed to the O-H stretching vibration of the hydroxyl functional groups of the cellulosic structure forming DFPP (Gündüz and Bayrak 2017). The two bands detected at 2,938 and $2,895\ cm^{-1}$ were assigned to (-CH) stretching vibrations in methylene ($-CH_2$) and methyl ($-CH_3$) in lignocellulosic groups, respectively (Thabede et al. 2020). The bands at 1,645 and $1,412\ cm^{-1}$ are due to symmetric and asymmetric stretching vibrations of $C=O$ in ionic carboxylic groups ($-COO^-$), respectively (Liang et al. 2010). The band at $1,328\ cm^{-1}$ can be attributed to the $C-O$ stretching vibrations in carboxylate groups (alkanes and alkyl groups) (Gündüz and Bayrak 2017). The band detected at $1,244\ cm^{-1}$ was assigned to the $C-O$ stretching vibration of the alcohol, phenol, ester, or ether groups (Sahu et al. 2020). The peak at $1,062\ cm^{-1}$ was attributed to the $C-O$ and $C-O-C$ vibrations and indicated the existence of cellulose, hemicellulose, and lignin in DFPP (Yang and Hong 2018). The band at $763\ cm^{-1}$ was attributed to $C-H$ out-of-plane bending in aromatics substituted by aliphatic
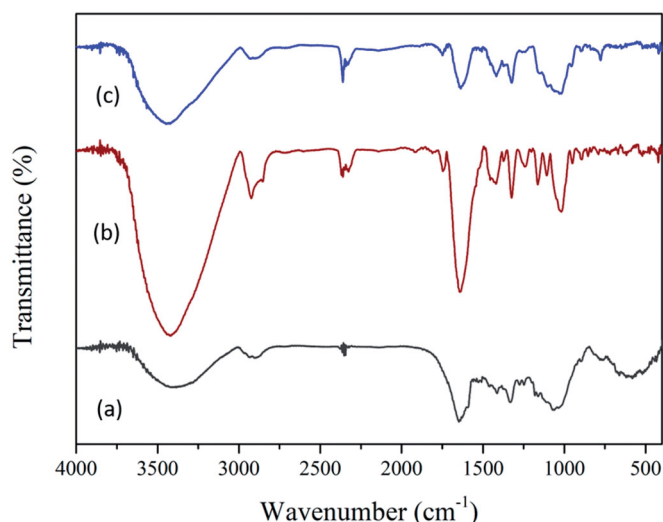

Figure 1. FT-IR spectrum of (a) DFPP, (b) CF-DFPP, and (c) RhB loaded CF-DFPP.

groups (Nuithitikul et al. 2010). After chemical treatment, some characteristic bands were shifted (3,409, 2,938, 2,895, 1,645, 1,412, 1,328, 1,243, 1,062, and $763\ cm^{-1}$ to 3,423, 2,921, 2,850, 1,638, 1,416, 1,321, 1,239, 1,017, and $789\ cm^{-1}$) and significant new bands in the CF-DFPP spectrum (Figure 1b) appeared at 1,742, 1,160, 1,106, and $946\ cm^{-1}$. The peak at $1,742\ cm^{-1}$ is the stretching vibration of the $C=O$ bond due to nonionic carboxyl groups ($-COOCH_3$, $-COOH$) and may be ascribed to carboxylic acids or their esters (Iqbal et al. 2009). The bands at 1,160 and 1,106 were assigned to the C-O stretch in the alcohol or ether or hydroxyl group (Achour et al. 2021). The peak at $946\ cm^{-1}$ can be assigned to the aromatic $-C-H$ bending vibrations (Mashkoor and Nasar 2019). These results proved that carboxyl groups had been successfully grafted onto DFPP by the etherification reaction with monochloroacetic acid. The FT-IR spectrum after RhB dye adsorption (Figure 1c) showed the bands are slightly shifted (3,423, 2,921, 1,742, 1,638, 1,416, 1,321, 1,106, 1,017, 946, and $789\ cm^{-1}$ to 3,432, 2,907, 1,749, 1,631, 1,420, 1,325, 1,102, 1,024, 953, and $775\ cm^{-1}$) and some bands are disappeared (2,850, 1,239, and $1,160\ cm^{-1}$), compared to the CF-DFPP spectrum (Figure 1b). These changes confirmed the interactions of RhB dye molecules with the CF-DFPP surface.

BET analysis

The BET analysis is one of the essential factors that regulate the adsorption efficiency of the biosorbent. Figure 2a,b show the N_2 adsorption-desorption isotherm plots of DFPP and CF-DFPP, which can be categorized as type-IV by IUPAC with an H_3 type hysteresis-loop (appearing in the relative pressure range of 0.4–1.0) (Eltaweil et al. 2020), indicating that DFPP and CF-DFPP have mesoporous structures. BET surface area, pore radius, and pore volume of the DFPP and CF-DFPP are summarized in Table 2. The surface area of DFPP is increased from 4.49 to $23.6\ m^2/g$ after carboxylate functionalization (From Table 2). This enhanced surface area of CF-DFPP will provide many active adsorption sites,
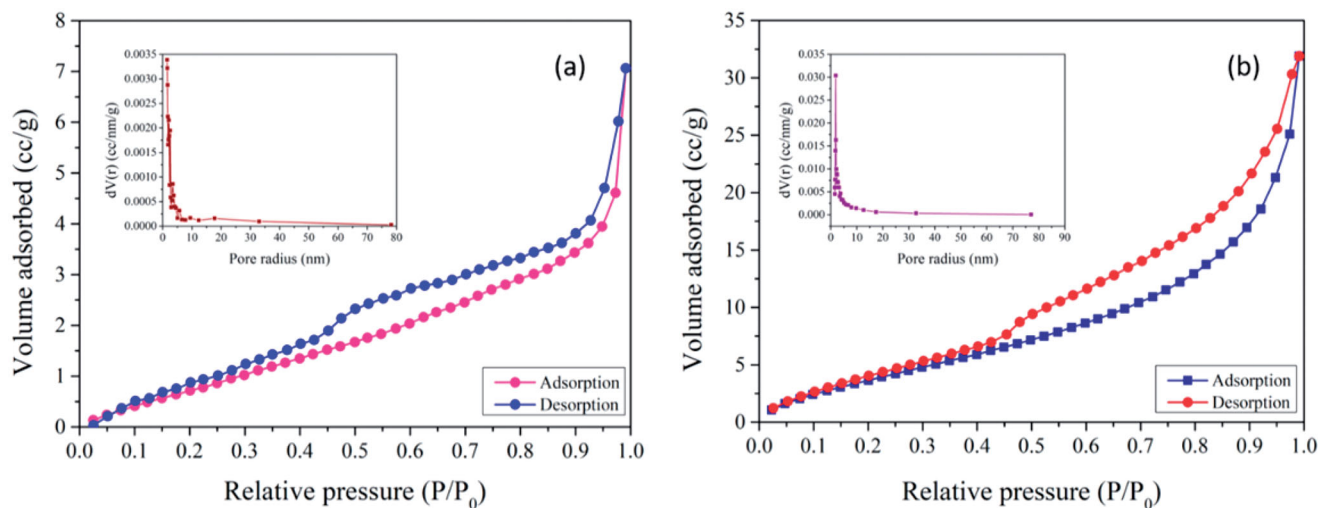
Figure 2. N_2 adsorption/desorption isotherms and BJH pore size distribution (inset of BET picture) of (a) DFPP and (b) CF-DFPP.

Table 2. Surface properties of DFPP and CF-DFPP.

Sample	BET surface area (m^2/g)	Pore volume (cc/g)	Pore radius (nm)
DFPP	4.49	0.011	1.49
CF-DFPP	23.55	0.052	2.27

resulting in higher pollutant adsorption capability. Moreover, the pore volume of DFPP also was risen from 0.011 to 0.052 cm^3/g after functionalization. Figure 2a,b (inset) display the pore size distribution of DFPP and CF-DFPP. The pore size distribution peaks of DFPP and CF-DFPP were centered at 1.49 and 2.13 nm, respectively. These results clarify that CF-DFPP has a large surface area and mesopores and could be used as an efficient biosorbent for removing pollutants from wastewater.

FE-SEM/EDX analysis

SEM analysis is commonly utilized to investigate the morphological features and surface properties of adsorbent materials. The surface morphology and elemental composition of DFPP, CF-DFPP, and RhB loaded CF-DFPP are presented in Figure 3. As seen in Figure 3a, the surface of DFPP was heterogonous, irregular in shape, and smooth. The CF-DFPP surface had a rough and irregular shape porous structure after carboxylate-functionalization (Figure 3b). The pores available in CF-DFPP facilitate the dye adsorption process because they provide a high internal surface area (Vigneshwaran *et al.* 2021b). After adsorption (Figure 3c), the CF-DFPP surface was completely covered by RhB dye, confirming the successful adsorption of RhB onto CF-DFPP. EDX analysis determines the elemental constitution of the adsorbents. The wt % of elements in DFPP (Figure 3d) are Carbon (44.6%), Oxygen (28.2%), Magnesium (6.7%), Potassium (15.9%) and Calcium (4.6%). In the CF-DFPP (Figure 3e), wt % of elements was found to be Carbon (51.1%), Oxygen (30.6%), Sodium (10.4%), Magnesium (2.6%), Chlorine (1.2%), Potassium (2.4%) and Calcium (1.7%). From the results, the CF-DFPP has a higher

percentage of carbon and oxygen compared to the DFPP, which will enhance dye adsorption. The weight % of elements in RhB loaded CF-DFPP (Figure 3f) are Carbon (49.8%), Oxygen (26.7%), Sodium (2.2%), and Calcium (21.3%). Some elements (Magnesium, Chlorine, and Potassium) disappeared after dye adsorption in the CF-DFPP. Moreover, changes in the elemental wt % values confirmed the successful adsorption of RhB on the surface of CF-DFPP.

Determination of pH_PZC of CF-DFPP

A solid addition method (Yadav *et al.* 2021) was used to evaluate the pH at the pH_{PZC} for CF-DFPP. Typically, 50 mL of NaCl (0.01 M) solution was transferred to a sequence of falcon tubes, and the pH was adjusted between 1.0 and 10.0 using 0.1 M NaOH and HCl. After achieving a consistent pH, 40 mg of biosorbent was added to the falcon tubes, and the solutions were stirred at 180 rpm at 298 K for 24 h. After filtering the suspensions, the pH of each sample was measured using a pH meter (S20-K, Mettler Toledo, USA). The $\Delta pH = pH_i$ (initial) – pH_f (final) and pH_i were plotted, with the point of intersection of the plot denoting the pH_{PZC} of the CF-DFPP.

Optimization of different parameters

Effect of pH

The pH of the solution determines and influences the adsorbate-adsorbent interaction. Figure 4a depicts the influence of the initial pH of the RhB solution on the removal rate. When seen in Figure 4a, the removal rate of CF-DFPP for RhB rose steadily from 27.8 to 94.1% as the pH climbed from 1.0 to 6.0. When the pH of the solution was higher than 6.0, there was no discernible difference in the adsorbent's removal effectiveness. The maximum removal rate of 94.1% was attained at pH 6.0. The protonation of RhB does not favor a significant rise in the elimination rate of the RhB dye under acidic circumstances. The positive
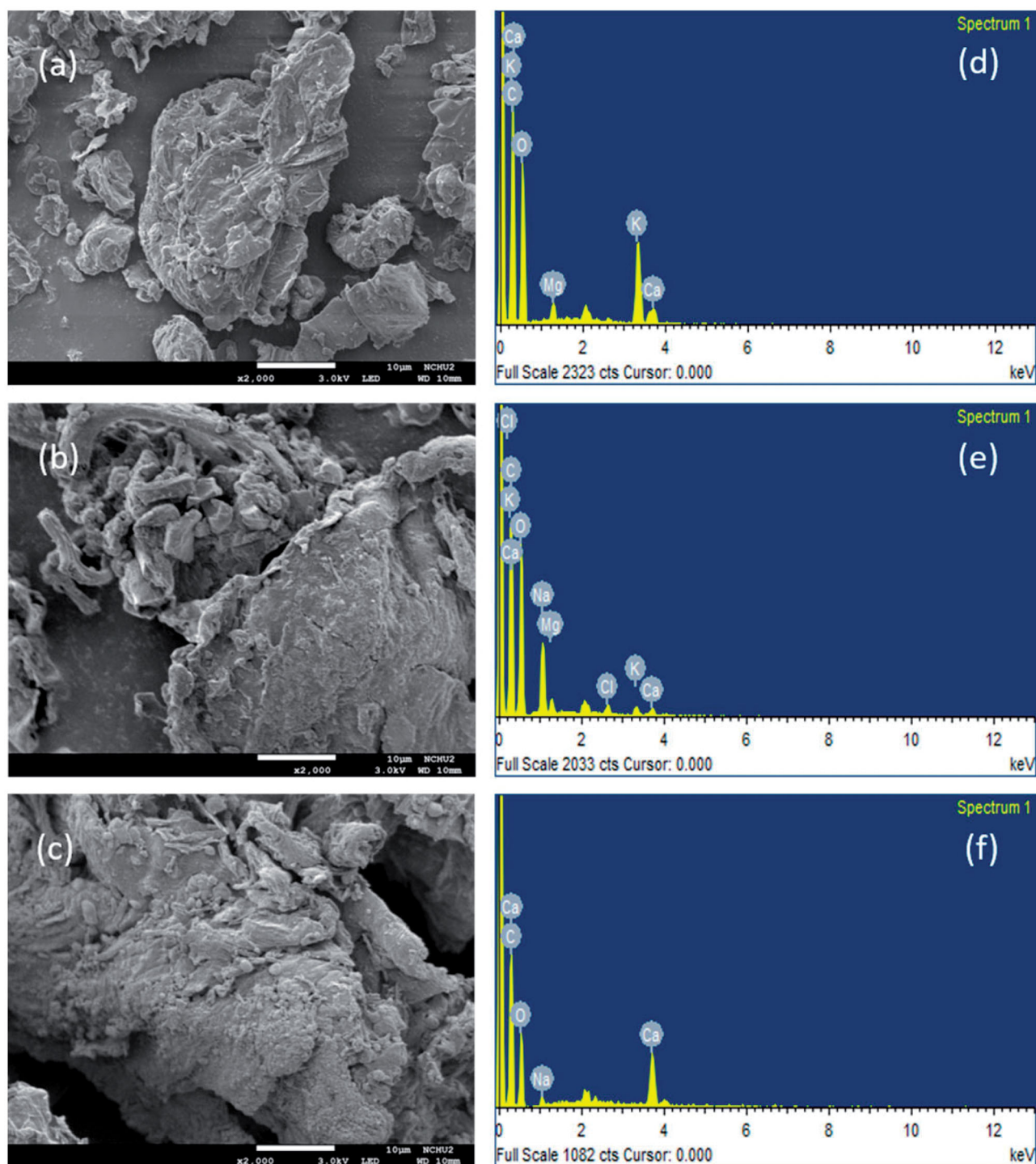
Figure 3. SEM images of (a) DFPP, (b) CF-DFPP, and (c) RhB loaded CF-DFPP; EDX spectrum of (d) DFPP, (f) CF-DFPP, and (f) RhB loaded CF-DFPP.

charge on the surface of the RhB dye competes with H^+ (hydroxide) ions and suffers electrostatic repulsion (Joshiba et al. 2021), resulting in poorer adsorption of RhB molecules by CF-DFPP. The fluctuating density of the RhB solution reduces as the pH rises, and the attractive electrostatic force between CF-DFPP and RhB increases, enhancing the adsorption activity. To further investigate the interaction between CF-DFPP and RhB molecules, pH_{PZC} of CF-DFPP was evaluated at various pH levels, as seen in Figure 4b.

When the pH is more than pH_{PZC}, the surface is negatively charged; the surface is positively charged when the pH is less than pH_{PZC}. The crossing point of the curve and zero line is around 5.8, as illustrated in Figure 4b, which is the pH_{PZC} of CF-DFPP. When the pH of CF-DFPP exceeds 6.0, the surface is negatively charged and easier to interact with cationic dyes (Ren et al. 2021). At an acidic pH, –COOH quickly ionizes to form $-COO^-$. In other words, at higher pH, the surface of CF-DFPP has a significant number of
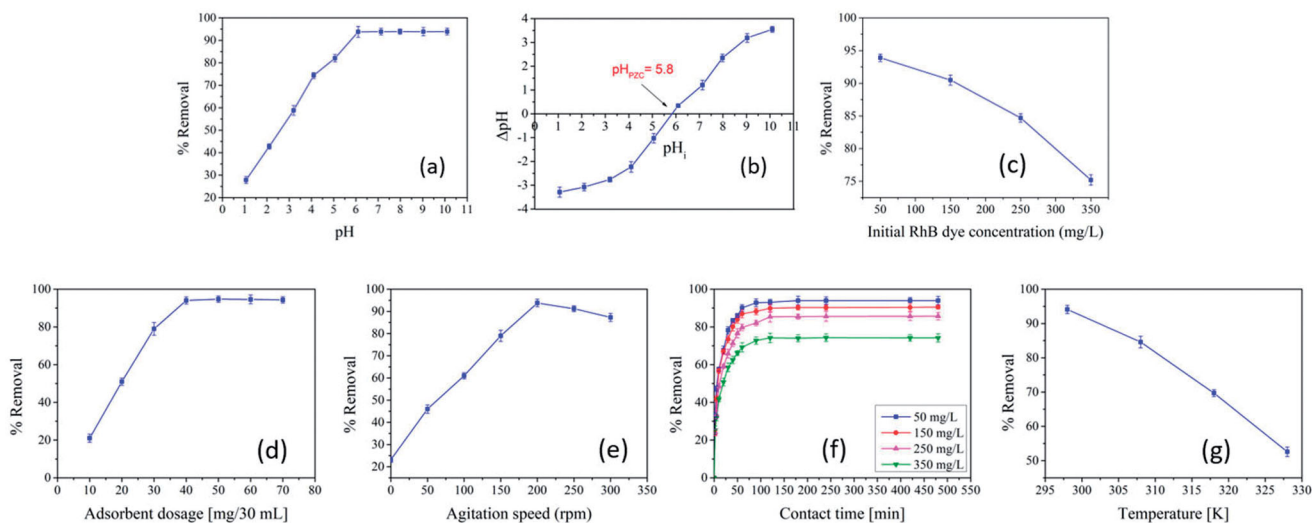
Figure 4. Effect of (a) solution of pH [pH: 1–10, dosage: 40 mg, C_o: 50 mg/L, V: 30 mL, speed: 200 rpm, time: 120 min, T: 298 K], (b) pH_{PZC} of CF-DFPP [pH: 1–10, electrolyte volume: 30 mL, dosage: 40 mg, speed: 120 rpm, time: 24 h, T: 298 K], (c) starting RhB dye concentration [C_o: 50–350 mg/L, pH: 6.0, dosage: 40 mg, V: 30 mL, speed: 200 rpm, T: 298 K], (d) adsorbent dosage [dosage: 10–70 mg, pH: 6.0, C_o: 50 mg/L, V: 30 mL, speed: 200 rpm, time: 120 min, T: 298 K], (e) agitation speed [speed: 0–300 rpm, C_o: 50 mg/L, pH: 6.0, dosage: 40 mg, V: 30 mL, T: 298 K], (f) contact time [C_o: 50–350 mg/L, dosage: 40 mg, pH: 6.0, V: 30 mL, speed: 200 rpm, T: 298 K], and (g) temperature [C_o: 50 mg/L, pH: 6.0, dosage: 40 mg, V: 30 mL, speed: 200 rpm, T: 298–328 K] for the RhB adsorption by CF-DFPP.

–COO⁻ binding sites (Ren *et al.* 2021), which is advantageous for RhB biosorption. These findings suggest that pH and electrostatic interactions play essential roles in the sorption process and significantly impact the interaction of biosorbent and dye. For further adsorption experiments pH of solutions was set to 6.0.

Starting RhB dye concentration

The impact of starting dye concentration on RhB removal by CF-DFPP is clearly demonstrated in Figure 4c. Adsorption tests are carried out in a variety of starting dye concentrations, including 50, 150, 250, and 350 mg/L in a constant biosorbent of around 40 mg/30 mL. The removal % of RhB decreases with increasing starting RhB dye concentration, as seen in Figure 4c. Initially, at low dye concentrations, the accessibility of the adsorption sites is somewhat high, indicating that the RhB may be easily adsorbed. Similarly, with increasing dye concentrations, there is a decrease in activation sites due to the obstruction of all available activation sites. The progressive rise in dye concentration causes increased concentration polarization around the activation sites, preventing additional RhB adsorption by CF-DFPP. As a result, the optimal starting dye concentration for subsequent experiments was determined to be 50 mg/L.

Influence of CF-DFPP amount

The adsorbent dosage is an essential factor in the adsorption process, and it has a considerable influence on the dye removal rate. The impact of sorbent dosage on the removal of RhB dye was tested at different amounts (10, 20, 30, 40, 50, 60, and 70 mg/30 mL) with other constant parameters such as pH of 6.0, starting RhB dye concentration of 50 mg/ L, temperature of 298 K, and duration of 120 min. Figure 4d depicts the influence of adsorbent mass on the % removal of

RhB dye from aqueous solutions. With an increase in adsorbent mass from 10 to 40 mg/30 mL, the removal efficiency of RhB rose from 21.3 to 94.1%. At 40 mg/30 mL, the maximum % removal of RhB dye (94.1%) was achieved. The rise in % removal might be attributed to an improvement in the adsorbent's surface as well as a rise in the number of active dye adsorption sites (Rajoriya *et al.* 2021). According to Figure 4d, dye adsorption rose rapidly up to 40 mg adsorbent dosage, after which there is no sudden rise or fall in the degree of adsorption due to the concentration polarization of pollutants on the adsorbent surface (Joshiba *et al.* 2021). As a result, 40 mg/30 mL was chosen as the optimal amount of adsorbent for further studies.

Agitation rate

Indeed, agitation speed is important in the adsorption process because it affects the amount of biosorbent/adsorbate interaction. The impact of RhB agitation speed on CF-DFPP was examined by altering the agitation speed from 0 to 300 rpm while holding the other parameters constant. The findings shown in Figure 4e demonstrated that the removal (%) rose from 23.2 to 93.8% when the agitation rate increased from 0 to 200 rpm and thereafter marginally decreased. Although increasing agitation speed causes more collisions between dye molecules and active sites, dye adsorption diminishes after 200 rpm. It may be said that after changing speeds after 200 rpm, the speed will be so quick that it limits and disrupts dye molecule absorption on active sites. As a result, the optimal agitation rate for RhB dye adsorption was 200 rpm, which was used for further research.

Effect of contact time

In an adsorption process, contact time is one of the critical factors that significantly influence adsorption efficiency. The
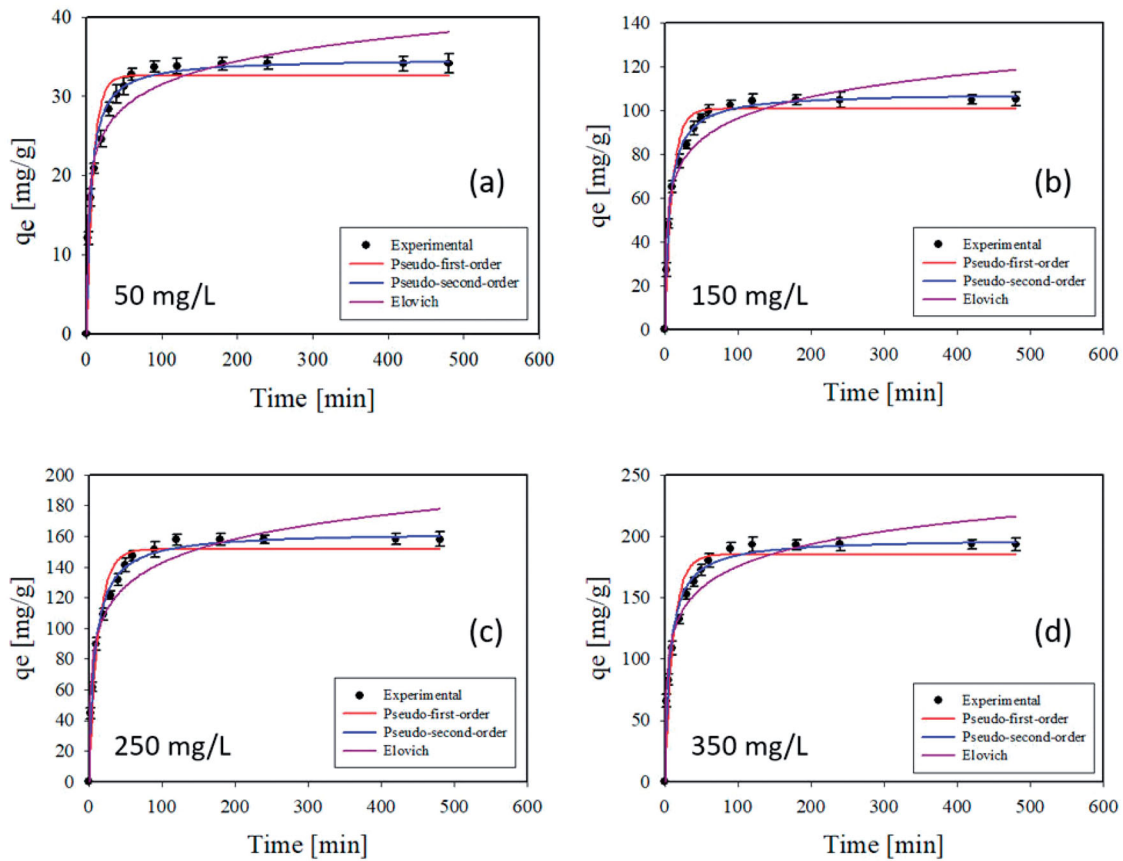
Figure 5. Non-linear plots of the PFO, PSO, and Elovich kinetic models for the RhB adsorption by CF-DFPP [C_o: 50–350 mg/L, dosage: 40 mg, pH: 6.0, V: 30 mL, speed: 200 rpm, T: 298 K].

optimal contact time was obtained by adjusting the contact time from 0 to 480 min for all four starting dye ion concentrations with a constant adsorbent dose throughout the adsorption tests. The mean contact time data are utilized to study the kinetics of RhB adsorption by CF-DFPP. The removal % steadily rises with increasing contact duration, as seen in Figure 4f. The optimum contact time for successful RhB adsorption was determined to be 120 min. Because of the abundance of adsorption activation sites, there is no steady rise in the elimination % of RhB after 120 min. It is obvious that a 120 min incubation period is more than enough for increased RhB elimination. At an optimum contact period of roughly 120 min, the highest removal % for 50, 150, 250, and 350 mg/L RhB on CF-DFPP seemed to be 93.9, 90.5, 85.7, and 74.2%. The adsorption of RhB onto the CF-DFPP was discovered to be smooth, single and continual, which drives the immersion and causes possible monolayer inclusion on the CF-DFPP surface. Hence, the contact time was fixed at 120 min for further experiments.

Adsorption kinetic studies

Adsorption reaction kinetics indicate the uptake rate until equilibrium, as well as the sorption behavior of the adsorption system. The kinetic reaction model uses time study data to predict the kind and sequence of reaction, which depicts the adsorbent's sorptive profile and efficiency.

Table 3. Calculated values of the kinetic parameters at various starting RhB dye concentrations.

Kinetic model	Parameters	Concentration of RhB solution (mg/L)			
		50	150	250	350
Experimental value	$q_{e,\ exp}$ (mg/g)	34.1	104.7	158.2	193.25
Pseudo-first-order	$q_{e1,\ cal}$ (mg/g)	35.29	100.57	151.48	185.11
	k_1 (1/min)	0.1134	0.0982	0.0775	0.0841
	R^2	0.9382	0.9642	0.9554	0.9356
Pseudo-second-order	$q_{e2,\ cal}$ (mg/g)	34.68	107.78	162.71	197.89
	k_2 (g/mg min)	0.0052	0.0014	0.0008	0.0007
	R^2	0.9855	0.9958	0.9908	0.9810
Elovich	α (mg/g min)	79.35	135.59	136.99	236.21
	β (g/mg)	0.2396	0.0713	0.0450	0.0388
	R^2	0.9445	0.9329	0.9448	0.9484

The extensively accepted reaction kinetic models, *i.e.*, PFO, PSO, and Elovich model, are employed in this work, and the model equations are as follows:

$$q_t = q_{e1}(1 - \exp(-k_1 t)) \qquad (4)$$

$$q_t = \frac{q_{e2}^2 k_2 t}{1 + q_{e2} k_2 t} \qquad (5)$$

$$q_t = \frac{1}{\beta} \ln(1 + \alpha \beta t) \qquad (6)$$

The fitting results of non-linearized PFO, PSO and Elovich kinetic models were displayed in Figure 5, and the

Table 4. Comparison of the adsorption performance of RhB dye with other reported adsorbents.

Adsorbent	pH	Starting dye concentration (mg/L)	Temperature (K)	Removal (%)	q_{max} (mg/g)	References
Magnetic lignin spheres	–	100–600	313	–	17.62	Li et al. (2016)
Magnetic lignosulfonate	–	30–250	298	–	22.47	Geng et al. (2019)
Trifunctional polyurethane/ graphene oxide electrospun membrane	–	–	–	–	77.15	Sundaran et al. (2019)
Fe₃O₄/Al pillared bentonite	–	10–60	298	98.7	62.15	Wan et al. (2015)
Beta zeolites with SiO₂/Al₂O	3.0	5–50	295	98.8	27.97	Cheng et al. (2018)
Dika nut char	3.0	50–300	299	81.82	52.9	Inyinbor et al. (2017)
Acid treated kaolinite	6.9	50–350	303	–	23.7	Bhattacharyya et al. (2014)
Microwave treated nilotica leaf	7.0	25–200	300	32.21	24.39	Santhi et al. (2014)
Sugarcane baggase	4.0	100–500	303	98	51.5	Zhang et al. (2013)
Biochar (bamboo shoot shells)	–	2–300	298	–	85.5	Hou et al. (2019)
Green microalgae	8.0	20–500	298	89	63.14	da Rosa et al. (2018)
Activated carbons (lignocellulosic waste)	7.0	65–140	318	99.85	39.98	da Silva Lacerda et al. (2015)
Eichhornia crassipes roots	4.0	5–60	293	60	27.15	Saufi et al. (2020)
Eichhornia crassipes leaves	4.0	5–60	293	63	44.60	Saufi et al. (2020)
Banana peel powder	4.0	5–25	303	81.07	3.88	Singh et al. (2018)
Tapioca peel waste	8.0	25–150	–	98	33.1	Vigneshwaran et al. (2021a)
CF-DFPP	6.0	50–400	298	94.2	228.7	Present study

derived variables are provided in Table 3. The experimental data can be best matched to the PSO model, which has the highest R^2 values (0.9908–0.9958) when compared to the PFO (0.9246–0.9642) and Elovich (0.9329–0.9484) models. Furthermore, the values of adsorption efficiency (q$_{e, cal}$) derived from the PSO model are closer to experimental values of adsorption efficiency (q$_{e, exp}$) than the values obtained from the other two models. As a consequence, the adsorption of RhB on CF-DFPP followed PSO kinetics, indicating that the rate-limiting step was not boundary layer resistance. The rate of dye adsorption may be greatly regulated by a chemisorption process in combination with the chemical properties of the adsorbent and dye (Barka et al. 2011). The Elovich model is used to characterize PSO and chemisorptive kinetics under the assumption that the surface of solid objects is energetically heterogeneous. The amplitude of α positively varied and β negatively varied with the RhB concentration (Table 3) confirming the chemisorptive type of RhB dye adsorption using the CF-DFPP.

Adsorption isotherm modeling

The number of adsorbate molecules adsorbed and the equilibrium concentration of an ion in the bulk of the solution are correlated using various adsorption isotherms. Different isothermal models, such as D-R, Freundlich, and Langmuir, were used to determine the amount of adsorption on the biosorbent surface at equilibrium pressure and constant temperature.

The Langmuir model is based on the premise that adsorption energy remains constant regardless of surface coverage. Adsorption efficiency may be achieved by forming a monolayer of adsorbate molecules on the biosorbent surface. This model non-linear equation may be written as follows:

$$q_e = \frac{q_{max} K_L C_e}{1 + K_L C_e} \quad (7)$$

Based on Langmuir, the maximum adsorption capability of CF-DFPP for RhB dye was found to be 228.7 mg/g at 298 K. Table 4 shows the adsorption capability of CF-DFPP with many biosorbents previously described in the literature for the elimination of RhB. When compared to the other sorbents described in Table 4, the dye molecule's adsorption capability on CF-DFPP was very high. As a result of Table 4, the CF-DFPP was suggested as a promising biosorbent material for eliminating RhB from an aqueous environment.

The dimensionless equilibrium parameter (called separation factor), R_L, is one of the key aspects of the Langmuir isotherm, as shown below:

$$R_L = \frac{1}{(1 + K_L C_o)} \quad (8)$$

The value of R_L shows whether the adsorption is irreversible ($R_L = 0$), unfavorable ($R_L > 1$), favorable ($0 < R_L < 1$), and linear ($R_L = 1$) (Chai et al. 2020). From Table 5 the calculated R_L values lie between 0 and 1 indicating the favorable condition of the isotherm for all concentrations.

For multilayer adsorption on heterogeneous surfaces, the Freundlich model is commonly utilized. The Freundlich model has also been used to explain multilayer adsorption's diffused mechanism. The non-linear expression of this model is represented as:

$$q_e = K_f C_e^{1/n} \quad (9)$$

The factor *1/n* has been used to represent the kind of adsorption's favorability. When the value of *1/n* is less than

Table 5. The calculated parameters of the isotherms and separation factors for the RhB adsorption by CF-DFPP at 298 K.

Adsorption isotherm	Parameter	Value
Langmuir	q_m (mg/g)	228.7
	K_L (L/mg)	0.052
	R^2	0.9993
	χ^2	4.28
Freundlich	K_f (mg/g)	36.31
	n	2.74
	$1/n$	0.365
	R^2	0.9712
	χ^2	165.1
Dubinin-Radushkevich	q_s (mg/g)	176.8
	K (mol^2/J^2)	0.0113
	E (kJ/mol)	6.65
	R^2	0.8476
	χ^2	626.9
Separation factor (R_L)	C_o (mg/L)	R_L
	50	0.28
	100	0.16
	150	0.11
	200	0.09
	250	0.07
	300	0.06
	350	0.052
	400	0.046

Figure 6. Non-linear isotherm plots for the RhB adsorption by CF-DFPP [C_o: 50–400 mg/L, dosage: 40 mg, pH: 6.0, V: 30 mL, speed: 200 rpm, T: 298 K].

0.5, the adsorbate is quickly adsorbed, and when the value is more than 2, the adsorbate is barely adsorbed (Chen *et al.* 2019). The $1/n$ value in this investigation was less than 0.5, suggesting that RhB adsorption onto CF-DFPP in the Freundlich model was favorable.

The D-R model is often used to explain the sorption process onto a heterogeneous surface with Gaussian energy distribution. The D-R model is described in its non-linear form as follows:

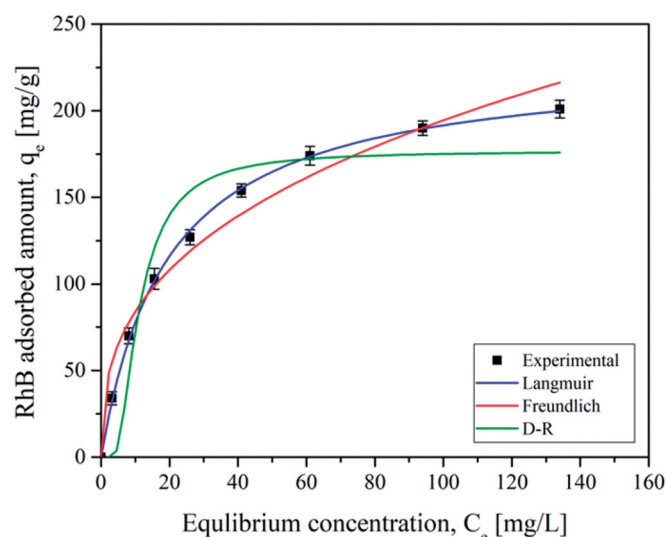$$q_e = q_s \exp\left(-K\varepsilon^2\right) \quad (10)$$

$$\varepsilon = RT \ln\left(1 + \frac{1}{C_e}\right) \quad (11)$$

The constant K provides the mean free energy, E (kJ/mol), of sorption per molecule of adsorbate when it is transported to the surface of the solid form infinite in the solution, which may be computed using the following expression:

$$E = \frac{1}{\sqrt{2K}} \quad (12)$$

By observing the value of E, the mechanism of adsorption may be predicted. When E is between 1.0 and 8.0 kJ/mol, the removal of adsorbate is considered to be the consequence of physical interactions, whereas E between 8.0 and 16.0 kJ/mol suggests a combination of adsorbate and biosorbent that relies on ion-exchange, and E more than 16.0 kJ/mol implies a chemisorption process (Yang *et al.* 2021). In the current study, the value of E is 0.633 kJ/mol, derived from Table 5, indicating that the dye ions are adsorbed through the physisorption process.

The correlation coefficients, R^2, and the Chi-square (χ^2) test were also employed to determine the best match among the adsorption isotherm models utilized. The following equation will be employed to evaluate the best-match model:

$$\chi^2 = \sum_{i=1}^{n}\left(\frac{(q_{e,\exp} - q_{e,cal})^2}{q_{e,cal}}\right) \quad (13)$$

The fitting curves of isotherms are shown in Figure 6, and the acquired constants from these models are shown in Table 5. The non-linear R^2 and χ^2 values for the three adsorption isotherms demonstrate that the Langmuir model seems to be the best-fitting model for the CF-DFPP adsorption isotherm data since it has the largest R^2 (0.999) and lowest χ^2 (0.126) values. This observation implies that dye ion binding can occur as a monolayer on the adsorbent surface and that monolayer adsorption takes place on a homogeneous surface.
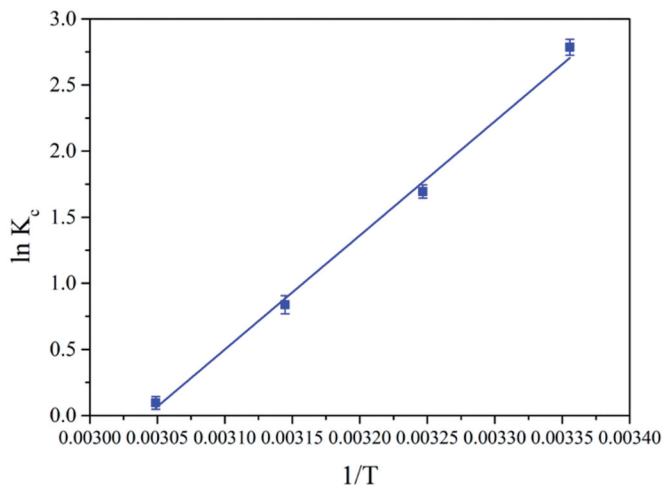
Effect of temperature and thermodynamics

Temperature is one of the significant factors that influence the sorption process. The effect of temperature on the adsorption of RhB on CF-DFPP was analyzed in the range of 298–328 K. As shown in Figure 4g, a conspicuous gradual decrease in the removal efficiency from 94.1 to 52.6% was occurred by raising the temperature from 298 to 328 K, which indicates that the adsorption RhB onto CF-DFPP is an exothermic and moreover is favorable at low temperature. A higher temperature would increase the solubility and mobility of RhB dye molecules during the adsorption process and decrease the adsorbent-adsorbate interactions owing to the high kinetic energy of the components, resulting in a drop in adsorption efficiency (Dai *et al.* 2021).

Thermodynamic investigations may provide further information on the inherent energy shifts involved with adsorption. In order to properly understand the adsorption thermodynamics of RhB on CF-DFPP, three essential thermodynamic variables, namely entropy change (ΔS^o), enthalpy change (ΔH^o), and Gibbs free energy change (ΔG^o), were studied in this work. The values of these thermodynamic variables were calculated using the following

Table 6. Thermodynamic parameters for the adsorption of RhB by CF-DFPP.

Temperature [K]	Thermodynamic parameters		
	ΔG^o (kJ/mol)	ΔS^o (J/mol K)	ΔH^o (kJ/mol)
298	−6.9001		
308	−4.3373	−221	−72.7
318	−2.2136		
328	−0.2599		

Figure 7. Van't Hoff plot for the RhB adsorption by CF-DFPP.

Equations:

$$\Delta G^o = \Delta H^o - T\Delta S^o \qquad (14)$$

$$\Delta G^o = -RT \ln K_c \qquad (15)$$

$$K_c = \frac{C_{Ae}}{C_e} \qquad (16)$$

$$\ln K_c = -\frac{\Delta G^o}{RT} = -\frac{\Delta H^o}{RT} + \frac{\Delta S^o}{R} \qquad (17)$$

The calculated thermodynamic variables and constants are given in Table 6. The ΔH^o and ΔS^o values can be determined by the slope and intercept of the curve of *1/T* versus *ln K_c* (Figure 7). The −ve values of ΔG^o at all temperatures imply that the adsorption of RhB on CF-DFPP is spontaneous. When the temperature was raised from 298 to 328 K, the ΔG^o values rose (Table 6). This indicates that when the temperature rises, the spontaneity of the sorption process will diminish (Eslek Koyuncu and Okur 2021). The adsorption process is simplified when the value of Gibbs free energy reduces with temperature, and the chemisorption process is involved when the Gibbs energy value is between −80 and −400 kJ/mol. However, in the current study, Gibbs' free energy values are < −20 kJ/mol, indicating the physical characteristics of the adsorption process (Saravanan *et al.* 2020). The −ve value of ΔH^o (−72.7 kJ/mol) indicates that the adsorption process progressed favorably at lower temperatures and that the sorption process is exothermic. This observation may be due to the weakening of bonds between adsorbate molecules and adsorbent active sites at high temperatures (Jawad *et al.* 2019). On the other hand, the −ve value of ΔS^o (−221 J/mol K) demonstrates a reduction in the system's randomness, which is another evidence of the exothermicity of the sorption process (Mallakpour and Tabesh 2021).

Desorption and regeneration studies

The adsorbent's adsorption-regeneration capability is a critical role play in its application in practical wastewater treatment. Recycling the adsorbent saves resources while also lowering secondary pollutants in the environment. The desorption tests were carried out using different eluents, such as H_2O, 0.1 M NaOH, 0.1 M HCl, 0.1 M CH_3COOH, and 0.1 M NaCl to remove the adsorbed dye molecules on the surface of the CF-DFPP. As shown in Figure 8a, NaOH showed a higher desorption efficiency of 96.8%, while the use of H_2O, CH_3COOH, NaCl, and HCl resulted in low desorption efficiency 28.4, 47.3, 69.6, and 81.1%, respectively. As a result, 0.1 M NaOH was selected as the best desorbing agent. Similarly, the desorption tests were performed with 0.1 M NaOH at various temperatures and the results are shown in Figure 8b. The desorption efficiency gradually decreases from 96.8 to 89.4% when the temperature of the solution is increase from 298 to 328 K, respectively. Therefore, the temperature of 298 K was chosen and maintained throughout the studies.

Furthermore, the six regeneration cycles were carried out with the 0.1 M NaOH eluent. Figure 8c depicts the adsorption/desorption efficiency percentages. Adsorption efficiency was 94.2% in the first cycle and decreased somewhat in subsequent cycles, reaching 83.4% in the fifth cycle. However, the adsorption efficiency decreased further in the sixth cycle, with an equilibrium adsorption efficiency of 81.7% detected, although the CF-DFPP remained very stable even after the sixth cycle of the regeneration study. The decline in dye removal effectiveness was caused by a number of factors, including weak electrostatic interactions between the biosorbent and the adsorbate, saturation of binding sites, persistent adsorbent denaturation, and changes in morphological features after repeated use. The desorption efficiency followed a pattern comparable to the adsorption efficiency. After achieving a desorption efficiency of 96.8% in the first cycle, the desorption efficiency steadily decreased to 87.6% after the sixth cycle of desorption. Thus, the findings showed that CF-DFPP has a remarkable regeneration capability and may be used for six consecutive adsorption-desorption cycles.

Adsorption mechanism

It is generally understood that the adsorption surface feature is critical in the adsorption process. Because of the presence of the carboxylate group, the adsorbent's structure was negatively charged. The RhB dye molecules were linked to the surface of CF-DFPP through electrostatic interactions based on adsorption experiments (the effect of pH). Because of the strong electrostatic interaction between anionic biosorbent and cationic RhB dye at high pH, the carboxyl groups on the adsorbent's surface were completely ionized. As a consequence, when compared to other adsorbents, the CF-DFPP displayed better adsorption of RhB (Table 4). Figure 9
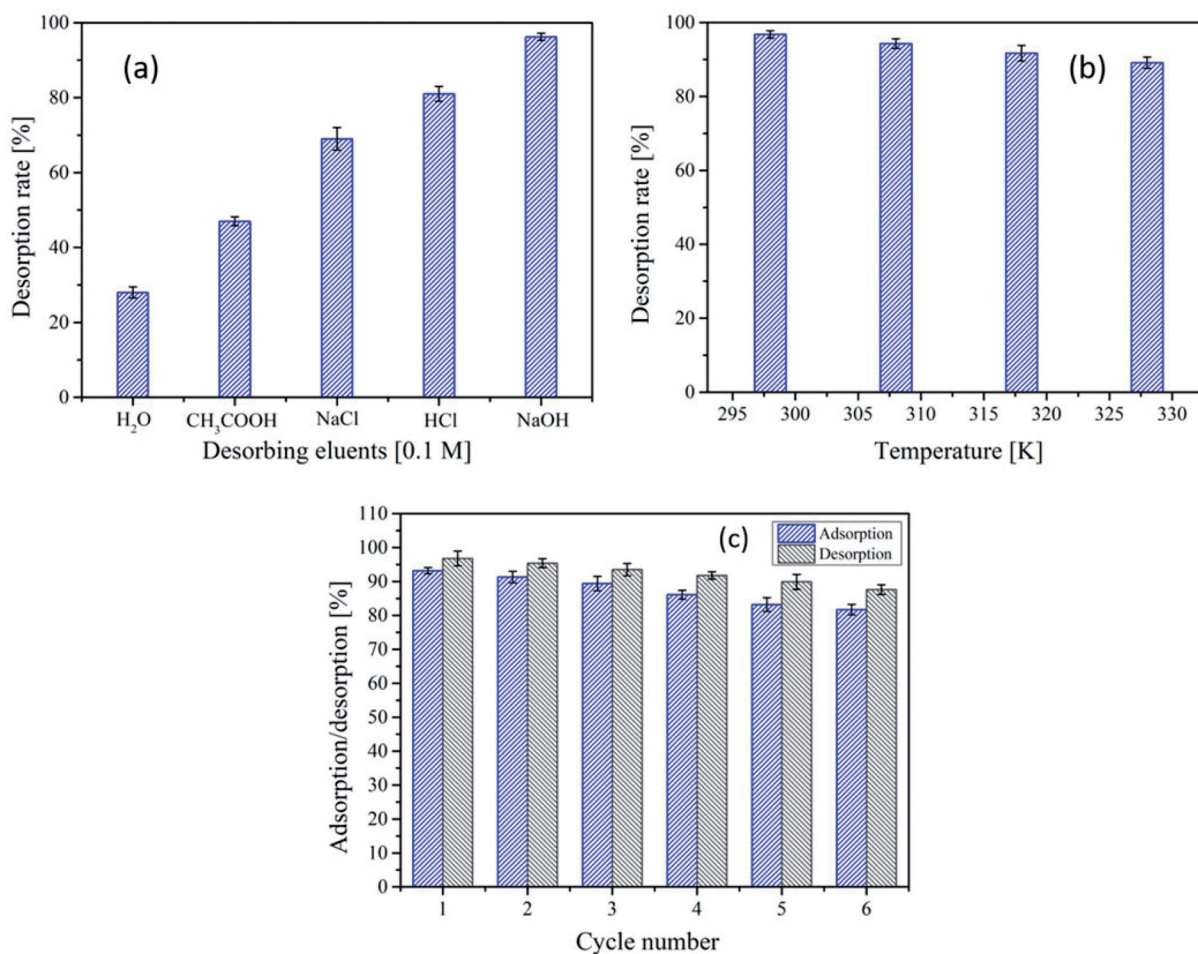
Figure 8. (a) Desorption of RhB adsorbed on CF-DFPP [desorbing eluent: 30 mL, speed: 200 rpm, time: 120 min, T: 298 K], (b) Desorption of adsorbed RhB using 0.1 M NaOH at different temperatures [desorbing eluent: 30 mL, speed: 200 rpm, time: 120 min, T: 298–328 K] and (c) Adsorption-desorption behavior of CF-DFPP [C_o: 50 mg/L, pH: 6.0, dosage: 40 mg, V: 30 mL, speed: 200 rpm, time: 120 min, T: 298 K].
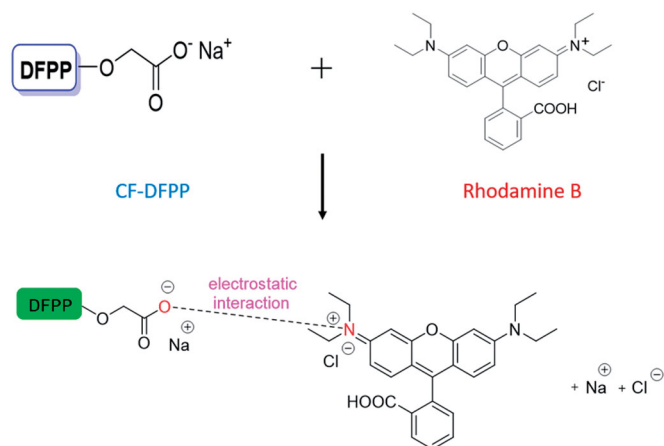

Figure 9. The possible adsorption mechanism of RhB onto CF-DFPP.

depicts the most plausible mechanism of CF-DFPP and its interaction with RhB molecules.

Conclusions

This study confirmed that a simple, low-toxic procedure using monochloroacetic acid could be feasibly used to prepare CF-DFPP. Chemical modification could significantly enhance the RhB removal ability of DFPP by increasing the adsorption sites on the surface due to the introduction of carboxylate functional groups. The RhB adsorption process was influenced by pH edge, temperature, adsorbent mass, stirring speed, contact time, and starting dye concentration. Various instrumental techniques such as FT-IR, FE-SEM/ EDX, pH_{PZC}, and BET analysis were utilized to characterize the DFPP, CF-DFPP, and RhB loaded CF-DFPP. The kinetic analysis implied that the adsorption of RhB onto CF-DFPP was well fitted by the PSO model ($R^2 > 0.9810$), which indicated that the dominant adsorption probably belonged to the chemisorptive nature. The adsorption isotherm models depicted that the Langmuir model ($R^2 = 0.9993$) was the best to describe the adsorption of RhB by CF-DFPP, demonstrating that the process involved monolayer adsorption with maximum coverage of 228.7 mg/g at 298 K. Moreover, adsorption of RhB onto CF-DFPP was pH-dependent and the optimal pH value was found to be 6.0. The thermodynamic analysis demonstrates that the RhB adsorption process with CF-DFPP is spontaneous, exothermic, and feasible in nature and lower temperature makes the adsorption process more favorable. After six adsorption/desorption cycles, the CF-DFPP maintained high adsorption efficiency,

indicating its promising recyclability. The electrostatic interactions played a vital role in the RhB adsorption mechanism. Based on the aforementioned experimental findings, CF-DFPP is the best candidate for being an effective adsorbent to remove RhB from water/wastewater due to its great adsorptive activity.

Funding

ORCID

Chi-Min Shu 🆔 http://orcid.org/0000-0001-9455-6162

References

Achour Y, Bahsis L, Ablouh EH, Yazid H, Laamari MR, Haddad ME. 2021. Insight into adsorption mechanism of Congo red dye onto Bombax Buonopozense bark activated-carbon using central composite design and DFT studies. Surfaces Interfaces. 23:100977. doi:10.1016/j.surfin.2021.100977.

Ahmad MA, Eusoff MA, Adegoke KA, Bello OS. 2021. Sequestration of methylene blue dye from aqueous solution using microwave assisted dragon fruit peel as adsorbent. Environ Technol Innov. 24:101917. doi:10.1016/j.eti.2021.101917.

Ahmad R, Ansari K. 2020. Chemically treated *Lawsonia inermis* seeds powder (CTLISP): an eco-friendly adsorbent for the removal of brilliant green dye from aqueous solution. Groundw Sustain Dev. 11: 100417. doi:10.1016/j.gsd.2020.100417.

Akpomie KG, Conradie J. 2021. Biosorption and regeneration potentials of magnetite nanoparticle loaded solanum tuberosum peel for celestine blue dye. Int J Phytoremediation. 23(4):347–361. doi:10.1080/15226514.2020.1814198.

Barka N, Abdennouri M, Makhfouk MEL. 2011. Removal of methylene blue and Eriochrome Black T from aqueous solutions by biosorption on Scolymus hispanicus L.: kinetics, equilibrium and thermodynamics. J Taiwan Inst Chem Eng. 42(2):320–326. doi:10.1016/j.jtice.2010.07.004.

Bhattacharyya KG, SenGupta S, Sarma GK. 2014. Interactions of the dye, Rhodamine B with kaolinite and montmorillonite in water. Appl Clay Sci. 99:7–17. doi:10.1016/j.clay.2014.07.012.

Chai Z, Li C, Zhu Y, Song X, Chen M, Yang YL, Chen D, Liang X, Wu J. 2020. Arginine-modified magnetic chitosan: preparation, characterization and adsorption of gallic acid in sugar solution. Int J Biol Macromol. 165(Pt A):506–516. doi:10.1016/j.ijbiomac.2020.09.141.

Chan SL, Tan YP, Abdullah AH, Ong ST. 2016. Equilibrium, kinetic and thermodynamic studies of a new potential biosorbent for the removal of Basic Blue 3 and Congo Red dyes: pineapple (Ananas comosus) plant stem. J Taiwan Inst Chem Eng. 61:306–315. doi:10.1016/j.jtice.2016.01.010.

Chen S, Qin C, Wang T, Chen F, Li X, Hou H, Zhou M. 2019. Study on the adsorption of dyestuffs with different properties by sludge-rice husk biochar: adsorption capacity, isotherm, kinetic, thermodynamics and mechanism. J Mol Liq. 285:62–74. doi:10.1016/j.molliq.2019.04.035.

Cheng ZL, Li YX, Liu Z. 2018. Study on adsorption of rhodamine B onto Beta zeolites by tuning SiO_2/Al_2O_3 ratio. Ecotoxicol Environ Saf. 148:585–592. doi:10.1016/j.ecoenv.2017.11.005.

da Rosa ALD, Carissimi E, Dotto GL, Sander H, Feris LA. 2018. Biosorption of rhodamine B dye from dyeing stones effluents using the green microalgae Chlorella pyrenoidosa. J Clean Prod. 198: 1302–1310. doi:10.1016/j.jclepro.2018.07.128.

da Silva Lacerda V, López-Sotelo JB, Correa-Guimarães A, Hernández-Navarro S, Sánchez-Báscones M, Navas-Gracia LM, Martín-Ramos P, Martín-Gil J. 2015. Rhodamine B removal with activated carbons obtained from lignocellulosic waste. J Environ Manage. 155:67–76. doi:10.1016/j.jenvman.2015.03.007.

Dai H, Chen Y, Ma L, Zhang Y, Cui B. 2021. Direct regeneration of hydrogels based on lemon peel and its isolated microcrystalline cellulose: characterization and application for methylene blue adsorption. Int J Biol Macromol. 191:129–138. doi:10.1016/j.ijbiomac.2021.09.063.

Devi VS, Sudhakar B, Prasad K, Jeremiah Sunadh P, Krishna M. 2020. Adsorption of Congo red from aqueous solution onto *Antigonon leptopus* leaf powder: equilibrium and kinetic modeling. Mater Today Proc. 26:3197–3206. doi:10.1016/j.matpr.2020.02.715.

Dos Santos Escobar O, Ferraz De Azevedo C, Swarowsky A, Adebayo MA, Schadeck Netto M, Machado Machado F. 2021. Utilization of different parts of *Moringa oleifera* Lam. seeds as biosorbents to remove Acid Blue 9 synthetic dye. J Environ Chem Eng. 9(4): 105553. doi:10.1016/j.jece.2021.105553.

Egbosiuba TC, Abdulkareem AS, Kovo AS, Afolabi EA, Tijani JO, Auta M, Roos WD. 2020. Ultrasonic enhanced adsorption of methylene blue onto the optimized surface area of activated carbon: adsorption isotherm, kinetics and thermodynamics. Chem Eng Res Des. 153: 315–336. doi:10.1016/j.cherd.2019.10.016.

Eltaweil AS, Ali Mohamed H, Abd El-Monaem EM, El-Subruiti GM. 2020. Mesoporous magnetic biochar composite for enhanced adsorption of malachite green dye: characterization, adsorption kinetics, thermodynamics and isotherms. Adv Powder Technol. 31(3): 1253–1263. doi:10.1016/j.apt.2020.01.005.

Eslek Koyuncu DD, Okur M. 2021. Removal of AV 90 dye using ordered mesoporous carbon materials prepared via nanocasting of KIT-6: adsorption isotherms, kinetics and thermodynamic analysis. Sep Purif Technol. 257:117657. doi:10.1016/j.seppur.2020.117657.

Geng J, Gu F, Chang J. 2019. Fabrication of magnetic lignosulfonate using ultrasonic-assisted *in situ* synthesis for efficient removal of Cr(VI) and Rhodamine B from wastewater. J Hazard Mater. 375: 174–181. doi:10.1016/j.jhazmat.2019.04.086.

Gündüz F, Bayrak B. 2017. Biosorption of malachite green from an aqueous solution using pomegranate peel: equilibrium modelling, kinetic and thermodynamic studies. J Mol Liq. 243:790–798. doi:10.1016/j.molliq.2017.08.095.

Hou Y, Huang G, Li J, Yang Q, Huang S, Cai J. 2019. Hydrothermal conversion of bamboo shoot shell to biochar: preliminary studies of adsorption equilibrium and kinetics for rhodamine B removal. J Anal Appl Pyrolysis. 143:104694. doi:10.1016/j.jaap.2019.104694.

Inyinbor AA, Adekola FA, Olatunji GA. 2017. Liquid phase adsorptions of Rhodamine B dye onto raw and chitosan supported mesoporous adsorbents: isotherms and kinetics studies. Appl Water Sci. 7(5):2297–2307. doi:10.1007/s13201-016-0405-4.

Iqbal M, Saeed A, Zafar SI. 2009. FTIR spectrophotometry, kinetics and adsorption isotherms modeling, ion exchange, and EDX analysis for understanding the mechanism of Cd(2+) and Pb(2+) removal by mango peel waste. J Hazard Mater. 164(1):161–171. doi:10.1016/j.jhazmat.2008.07.141.

Jawad AH, Norrahma SSA, Hameed BH, Ismail K. 2019. Chitosan-glyoxal film as a superior adsorbent for two structurally different reactive and acid dyes: adsorption and mechanism study. Int J Biol Macromol. 135:569–581. doi:10.1016/j.ijbiomac.2019.05.127.

Joshiba GJ, Kumar PS, Govarthanan M, Ngueagni PT, Abilarasu A, Carolin C F. 2021. Investigation of magnetic silica nanocomposite immobilized Pseudomonas fluorescens as a biosorbent for the effective sequestration of Rhodamine B from aqueous systems. Environ Pollut. 269:116173. doi:10.1016/j.envpol.2020.116173.

Kamranifar M, Khodadadi M, Samiei V, Dehdashti B, Noori Sepehr M, Rafati L, Nasseh N. 2018. Comparison the removal of reactive red 195 dye using powder and ash of barberry stem as a low cost adsorbent from aqueous solutions: Isotherm and kinetic study. J Mol Liq. 255:572–577. doi:10.1016/j.molliq.2018.01.188.

Khorasani AC, Shojaosadati SA. 2019. Magnetic pectin-chlorella vulgaris biosorbent for the adsorption of dyes. J Environ Chem Eng. 7(3): 103062. doi:10.1016/j.jece.2019.103062.

Li Y, Wu M, Wang B, Wu Y, Ma M, Zhang X. 2016. Synthesis of magnetic lignin-based hollow microspheres: a highly adsorptive and reusable adsorbent derived from renewable resources. ACS Sustainable Chem Eng. 4(10):5523–5532. doi:10.1021/acssuschemeng. 6b01244.

Liang S, Guo X, Feng N, Tian Q. 2010. Isotherms, kinetics and thermodynamic studies of adsorption of Cu^{2+} from aqueous solutions by Mg^{2+}/K^+ type orange peel adsorbents. J Hazard Mater. 174(1–3): 756–762. doi:10.1016/j.jhazmat.2009.09.116.

Mallakpour S, Tabesh F. 2021. Effective adsorption of methylene blue dye from water solution using renewable natural hydrogel bionanocomposite based on tragacanth gum: linear-nonlinear calculations. Int J Biol Macromol. 187:319–324. doi:10.1016/j.ijbiomac.2021.07.105.

Mashkoor F, Nasar A. 2019. Preparation, characterization and adsorption studies of the chemically modified Luffa aegyptica peel as a potential adsorbent for the removal of malachite green from aqueous solution. J Mol Liq. 274:315–327. doi:10.1016/j.molliq.2018.10.119.

Mu B, Wang A. 2016. Adsorption of dyes onto palygorskite and its composites: a review. J Environ Chem Eng. 4(1):1274–1294. doi:10. 1016/j.jece.2016.01.036.

Munagapati VS, Wen JC, Pan CL, Gutha Y, Wen JH. 2019. Enhanced adsorption performance of reactive red 120 azo dye from aqueous solution using quaternary amine modified orange peel powder. J Mol Liq. 285:375–385. doi:10.1016/j.molliq.2019.04.081.

Naushad M, Alqadami AA, AlOthman ZA, Alsohaimi IH, Algamdi MS, Aldawsari AM. 2019. Adsorption kinetics, isotherm and reusability studies for the removal of cationic dye from aqueous medium using arginine modified activated carbon. J Mol Liq. 293:111442. doi:10.1016/j.molliq.2019.111442.

Nazir MA, Bashir MS, Jamshaid M, Anum A, Najam T, Shahzad K, Imran M, Shah SSA, ur Rehman A. 2021. Synthesis of porous secondary metal-doped MOFs for removal of Rhodamine B from water: role of secondary metal on efficiency and kinetics. Surfaces Interfaces. 25:101261. doi:10.1016/j.surfin.2021.101261.

Nuithitikul K, Srikhun S, Hirunpraditkoon S. 2010. Kinetics and equilibrium adsorption of Basic Green 4 dye on activated carbon derived from durian peel: effects of pyrolysis and post-treatment conditions. J Taiwan Inst Chem Eng. 41(5):591–598. doi:10.1016/j.jtice.2010.01.007.

Palamthodi S, Lele SS. 2016. Optimization and evaluation of reactive dye adsorption on bottle gourd peel. J Environ Chem Eng. 4(4): 4299–4309. doi:10.1016/j.jece.2016.09.032.

Pavan FA, Camacho ES, Lima EC, Dotto GL, Branco VTA, Dias SLP. 2014. Formosa papaya seed powder (FPSP): preparation, characterization and application as an alternative adsorbent for the removal of crystal violet from aqueous phase. J Environ Chem Eng. 2(1): 230–238. doi:10.1016/j.jece.2013.12.017.

Rajoriya S, Saharan VK, Pundir AS, Nigam M, Roy K. 2021. Adsorption of methyl red dye from aqueous solution onto eggshell waste material: kinetics, isotherms and thermodynamic studies. Curr Res Green Sustain Chem. 4:100180. doi:10.1016/j.crgsc.2021.100180.

Ren L, Tang Z, Du J, Chen L, Qiang T. 2021. Recyclable polyurethane foam loaded with carboxymethyl chitosan for adsorption of methylene blue. J Hazard Mater. 417:126130. doi:10.1016/j.jhazmat.2021. 126130.

Sadegh N, Haddadi H, Arabkhani P, Asfaram A, Sadegh F. 2021. Simultaneous elimination of Rhodamine B and Malachite Green dyes from the aqueous sample with magnetic reduced graphene oxide nanocomposite: optimization using experimental design. J Mol Liq. 343:117710. doi:10.1016/j.molliq.2021.117710.

Sahu S, Pahi S, Tripathy S, Singh SK, Behera A, Sahu UK, Patel RK. 2020. Adsorption of methylene blue on chemically modified lychee seed biochar: dynamic, equilibrium, and thermodynamic study. J Mol Liq. 315:113743. doi:10.1016/j.molliq.2020.113743.

Santhi T, Prasad AL, Manonmani S. 2014. A comparative study of microwave and chemically treated Acacia nilotica leaf as an eco friendly adsorbent for the removal of rhodamine B dye from aqueous solution. Arab J Chem. 7(4):494–503. doi:10.1016/j.arabjc.2010.11.008.

Saravanan A, Karishma S, Jeevanantham S, Jeyasri S, Kiruthika AR, Kumar PS, Yaashikaa PR. 2020. Optimization and modeling of reactive yellow adsorption by surface modified Delonix regia seed: study of nonlinear isotherm and kinetic parameters. Surfaces Interfaces. 20:100520. doi:10.1016/j.surfin.2020.100520.

Saufi H, Alouani ME, Aride J, Taibi M. 2020. Rhodamine B biosorption from aqueous solution using Eichhornia crassipes powders: isotherm, kinetic and thermodynamic studies. Chem Data Collect. 25: 100330. doi:10.1016/j.cdc.2019.100330.

Sharma G, Naushad M, Kumar A, Rana S, Sharma S, Bhatnagar A, Stadler FJ, Ghfar AA, Khan MR. 2017. Efficient removal of coomassie brilliant blue R-250 dye using starch/poly(alginic acid-cl-acrylamide) nanohydrogel. Process Saf Environ Prot. 109:301–310. doi: 10.1016/j.psep.2017.04.011.

Sharma G, Naushad M, Pathania D, Mittal A, El-desoky GE. 2015. Modification of Hibiscus cannabinus fiber by graft copolymerization: application for dye removal. Desalin Water Treat. 54(11):3114–3121. doi:10.1080/19443994.2014.904822.

Shehzad K, Xie C, He J, Cai X, Xu W, Liu J. 2018. Facile synthesis of novel calcined magnetic orange peel composites for efficient removal of arsenite through simultaneous oxidation and adsorption. J Colloid Interface Sci. 511:155–164. doi:10.1016/j.jcis.2017.09.110.

Siddiqui SI, Rathi G, Chaudhry SA. 2018. Acid washed black cumin seed powder preparation for adsorption of methylene blue dye from aqueous solution: thermodynamic, kinetic and isotherm studies. J Mol Liq. 264:275–284. doi:10.1016/j.molliq.2018.05.065.

Singh S, Parveen N, Gupta H. 2018. Adsorptive decontamination of rhodamine-B from water using banana peel powder: A biosorbent. Environ Technol Innov. 12:189–195. doi:10.1016/j.eti.2018.09.001.

Sukla Baidya K, Kumar U. 2021. Adsorption of brilliant green dye from aqueous solution onto chemically modified areca nut husk. South African J Chem Eng. 35:33–43. doi:10.1016/j.sajce.2020.11.001.

Sundaran SP, Reshmi CR, Sagitha P, Manaf O, Sujith A. 2019. Multifunctional graphene oxide loaded nanofibrous membrane for removal of dyes and coliform from water. J Environ Manage. 240: 494–503. doi:10.1016/j.jenvman.2019.03.105.

Thabede PM, Shooto ND, Xaba T, Naidoo EB. 2020. Adsorption studies of toxic cadmium(II) and chromium(VI) ions from aqueous solution by activated black cumin (Nigella sativa) seeds. J Environ Chem Eng. 8(4):104045. doi:10.1016/j.jece.2020.104045.

Vigneshwaran S, Sirajudheen P, Karthikeyan P, Meenakshi S. 2021a. Fabrication of sulfur-doped biochar derived from tapioca peel waste with superior adsorption performance for the removal of Malachite green and Rhodamine B dyes. Surfaces Interfaces. 23:100920. doi:10. 1016/j.surfin.2020.100920.

Vigneshwaran S, Sirajudheen P, Nikitha M, Ramkumar K, Meenakshi S. 2021b. Facile synthesis of sulfur-doped chitosan/biochar derived from tapioca peel for the removal of organic dyes: isotherm, kinetics and mechanisms. J Mol Liq. 326:115303. doi:10.1016/j.molliq.2021. 115303.

Wan D, Li W, Wang G, Chen K, Lu L, Hu Q. 2015. Adsorption and heterogeneous degradation of rhodamine B on the surface of magnetic bentonite material. Appl Surf Sci. 349:988–996. doi:10.1016/j. apsusc.2015.05.004.

Wang L, Wang Y, Ma F, Tankpa V, Bai S, Guo X, Wang X. 2019. Mechanisms and reutilization of modified biochar used for removal of heavy metals from wastewater: a review. Sci Total Environ. 668: 1298–1309. doi:10.1016/j.scitotenv.2019.03.011.

Wekoye JN, Wanyonyi WC, Wangila PT, Tonui MK. 2020. Kinetic and equilibrium studies of Congo red dye adsorption on cabbage waste powder. Environ Chem Ecotoxicol. 2:24–31. doi:10.1016/j.enceco. 2020.01.004.

Yadav S, Asthana A, Singh AK, Chakraborty R, Vidya SS, Susan MABH, Carabineiro SAC. 2021. Adsorption of cationic dyes, drugs and metal from aqueous solutions using a polymer composite of magnetic/β-cyclodextrin/activated charcoal/Na alginate: isotherm, kinetics and regeneration studies. J Hazard Mater. 409:124840. doi: 10.1016/j.jhazmat.2020.124840.

Yang JX, Hong GB. 2018. Adsorption behavior of modified Glossogyne tenuifolia leaves as a potential biosorbent for the removal of dyes. J Mol Liq. 252:289–295. doi:10.1016/j.molliq.2017.12.142.

Yang X, Zhu W, Song Y, Zhuang H, Tang H. 2021. Removal of cationic dye BR46 by biochar prepared from Chrysanthemum morifolium Ramat straw: a study on adsorption equilibrium, kinetics and isotherm. J Mol Liq. 340:116617. doi:10.1016/j.molliq.2021.116617.

Zhang Z, O'Hara IM, Kent GA, Doherty WOS. 2013. Comparative study on adsorption of two cationic dyes by milled sugarcane bagasse. Ind Crops Prod. 42:41–49. doi:10.1016/j.indcrop.2012.05.008.